Since January 2020 Elsevier has created a COVID-19 resource centre with free information in English and Mandarin on the novel coronavirus COVID-19. The COVID-19 resource centre is hosted on Elsevier Connect, the company's public news and information website.

Computers in Biology and Medicine 154 (2023) 106567

Contents lists available at ScienceDirect

Computers in Biology and Medicine

journal homepage: www.elsevier.com/locate/compbiomed

Classification of COVID-19 from community-acquired pneumonia: Boosting the performance with capsule network and maximum intensity projection image of CT scans

Yanan Wu [a,b], Qianqian Qi [c], Shouliang Qi [a,b,*], Liming Yang [d], Hanlin Wang [e], Hui Yu [f,**], Jianpeng Li [g], Gang Wang [g], Ping Zhang [h], Zhenyu Liang [i], Rongchang Chen [j]

[a] College of Medicine and Biological Information Engineering, Northeastern University, Shenyang, China
[b] Key Laboratory of Intelligent Computing in Medical Image, Ministry of Education, Northeastern University, Shenyang, China
[c] Research Center for Healthcare Data Science, Zhejiang Lab, Hangzhou, China
[d] Department of Radiology, The Affiliated Hospital of Guizhou Medical University, Guiyang, China
[e] Department of Radiology, General Hospital of the Yangtze River Shipping, Wuhan, China
[f] General Practice Center, The Seventh Affiliated Hospital, Southern Medical University, Guangzhou, China
[g] Department of Radiology, Affiliated Dongguan Hospital, Southern Medical University, Dongguan, China
[h] Department of Pulmonary and Critical Care Medicine, Affiliated Dongguan Hospital, Southern Medical University, Dongguan, China
[i] State Key Laboratory of Respiratory Disease, National Clinical Research Center for Respiratory Disease, Guangzhou Institute of Respiratory Health, The First Affiliated Hospital of Guangzhou Medical University, Guangzhou, China
[j] Key Laboratory of Respiratory Disease of Shenzhen, Shenzhen Institute of Respiratory Disease, Shenzhen People's Hospital (Second Affiliated Hospital of Jinan University, First Affiliated Hospital of South University of Science and Technology of China), Shenzhen, China

ARTICLE INFO

Keywords:
Maximum intensity projection
Capsule network
COVID-19
Community-acquired pneumonia
Computed tomography

ABSTRACT

Background: The coronavirus disease 2019 (COVID-19) and community-acquired pneumonia (CAP) present a high degree of similarity in chest computed tomography (CT) images. Therefore, a procedure for accurately and automatically distinguishing between them is crucial.
Methods: A deep learning method for distinguishing COVID-19 from CAP is developed using maximum intensity projection (MIP) images from CT scans. LinkNet is employed for lung segmentation of chest CT images. MIP images are produced by superposing the maximum gray of intrapulmonary CT values. The MIP images are input into a capsule network for patient-level pred iction and diagnosis of COVID-19. The network is trained using 333 CT scans (168 COVID-19/165 CAP) and validated on three external datasets containing 3581 CT scans (2110 COVID-19/1471 CAP).
Results: LinkNet achieves the highest Dice coefficient of 0.983 for lung segmentation. For the classification of COVID-19 and CAP, the capsule network with the DenseNet-121 feature extractor outperforms ResNet-50 and Inception-V3, achieving an accuracy of 0.970 on the training dataset. Without MIP or the capsule network, the accuracy decreases to 0.857 and 0.818, respectively. Accuracy scores of 0.961, 0.997, and 0.949 are achieved on the external validation datasets. The proposed method has higher or comparable sensitivity compared with ten state-of-the-art methods.
Conclusions: The proposed method illustrates the feasibility of applying MIP images from CT scans to distinguish COVID-19 from CAP using capsule networks. MIP images provide conspicuous benefits when exploiting deep learning to detect COVID-19 lesions from CT scans and the capsule network improves COVID-19 diagnosis.

* Corresponding author. College of Medicine and Biological Information Engineering, Northeastern University, Shenyang, China.
** Corresponding author.
E-mail addresses: 2010478@stu.neu.edu.cn (Y. Wu), 386489753@qq.com (Q. Qi), qisl@bmie.neu.edu.cn (S. Qi), 964310978@qq.com (L. Yang), 75288763@qq.com (H. Wang), 331693861@qq.com (H. Yu), 106443688@qq.com (J. Li), 13711982022@139.com (G. Wang), dgzp688@qq.com (P. Zhang), 490458234@qq.com (Z. Liang), chenrc@vip.163.com (R. Chen).

https://doi.org/10.1016/j.compbiomed.2023.106567
Received 30 October 2022; Received in revised form 30 December 2022; Accepted 22 January 2023
Available online 23 January 2023

1. Introduction

Coronavirus disease 2019 (COVID-19) was first observed in humans in late 2019 and has since spread across the globe [1,2]. The real-time polymerase chain reaction (RT-PCR) test is the gold standard for diagnosing COVID-19 through the detection of the novel coronavirus nucleic acid [3]. The PCR results of patients affected by detoxification concentration always show a false negative, with multiple nucleic-acid tests required to confirm the diagnosis [4,5]. Computed tomography (CT) images are used to detect and diagnose chest lesions, such as ground-glass opacities and crazy-paving [6–8]. However, in CT images, community-acquired pneumonia (CAP) and COVID-19 appear similar, and it is challenging to distinguish them, even for experienced radiologists.

Deep learning methods, especially convolutional neural networks (CNNs), have significant feature representation abilities and provide effective tools in diagnosing COVID-19 and distinguishing COVID-19 from CAP through computer-aided systems via chest X-rays and CT images. Rahaman et al. [1] investigated 15 different state-of-the-art pre-trained CNN models, including VGG, ResNet, InceptionNets, DenseNets, MobileNet, and Xception, for recognizing COVID-19 from chest X-rays. Moreover, a combination of DarkNet and AlexNet [9] and a pretrained DenseNet-121 model [10] have been used to diagnose COVID-19 patients using chest X-rays. In contrast to chest X-rays, CT images allow more details to be obtained with no overlapping tissues and provide an effective tool for distinguishing COVID-19 from CAP. Three-dimensional (3D) volume analysis and two-dimensional (2D) slice analysis have been combined to provide CT images for the classification of COVID-19 and CAP [11]. Qi et al. [12] proposed a multiple-instance learning method to distinguish COVID-19 from CAP, while Qi and his colleagues [13] developed a fully automatic deep-learning pipeline that can accurately distinguish COVID-19 from CAP using CT images by mimicking the diagnostic process of radiologists. On the basis of the above methods, more robust and advanced deep-learning models should be developed to improve the diagnosis of COVID-19.

Although deep learning using CT images and chest X-rays achieves high-accuracy diagnosis and classification of COVID-19 from CAP, few studies take the routine workflow of radiologists into account. A more effective and explainable procedure is required given the high degree of similarity between chest CT images of COVID-19 and CAP. Initially, radiologists in clinical practice quickly scan maximum intensity projection (MIP) images to identify lesion candidates (high-CT-value region) for additional testing on particular slices. Inspired by this procedure, we propose a novel CNN-based method that uses MIP images from CT scans and a capsule network. The purpose of this study is to explore whether MIP images generated from CT scans could help capsule networks to improve performance in terms of distinguishing COVID-19 from CAP and enhance the efficiency of COVID-19 diagnosis.

Histological studies have demonstrated that the pulmonary vasculature is affected by pneumonia, and that a high prevalence of thromboembolic disease is a hallmark of severe COVID-19 infection [14]. Existing studies have focused on the lung parenchymal involvement of CT imaging features, with few studies exploring the role of the pulmonary vascular system in COVID-19 [15]. A previous study indicates that the pulmonary vascular system in COVID-19 is redistributed from smaller to larger vessels [16].

MIP [17] is a widely used postprocessing technique for CT images, such as in the detection of lung nodules, for which it enhances the visualization [18]. An MIP image is a two-dimensional representation acquired using the fluoroscopic method, which means that it is obtained by calculating the maximum density of pixels that pass over each ray of the object. In CT imaging, when X-rays pass through a section of raw tissue, the pixel value with the highest density along this camera direction is retained and projected onto a two-dimensional plane to obtain a reconstructed MIP image, as shown in Fig. 1. Therefore, the MIP technique provides an excellent response for representing the vascular morphology. MIP images can show even small density changes, accurately reflect the condition of blood vessels, and can distinguish the calcification of vessel walls. In our method, MIP is used to identify changes in the vascular morphology and determine the presence of lesions in CT images. Some examples of CT scans in COVID-19 and CAP patients using the MIP method are shown in Fig. 2.

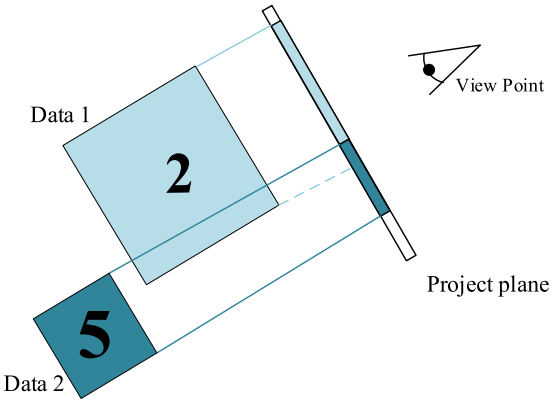

Fig. 1. Schematic overview of MIP rendering. The maximum intensities along rays originating in the viewpoint are projected.

In this paper, we describe a DenseNet-121-based capsule network for distinguishing COVID-19 from CAP using MIP images generated from CT scans. Excellent performance is achieved on multi-center datasets. The main contributions of this work are as follows. (1) We annotate lung masks of COVID-19 cases and train LinkNet to segment these masks. (2) MIP images are produced by superposing the maximum gray of intrapulmonary CT values to represent the morphological changes in vessels and lesions of COVID-19. (3) We propose an MIP-based framework for distinguishing COVID-19 from CAP. (4) We demonstrate the feasibility of combining the clinical screening method and capsule network to improve the performance of distinguishing COVID-19 from CAP and enhance the diagnosis of COVID-19.

The remainder of this paper is organized as follows. Section 2 introduces multiple CT image datasets, and gives an overview of the proposed method, lung segmentation, MIP image acquisition, and the capsule network. An ablation study and details of the training and evaluation of models are also described in Section 2. Section 3 presents the ablation experiment results, discusses the performance of the proposed method on multiple datasets, and compares the proposed method with state-of-the-art COVID-19 classification methods. Section 4 discusses the challenges of lung segmentation in COVID-19 cases, and outlines the advantages of the proposed method, its limitations, and future work. Finally, Section 5 summarizes the proposed model and suggests ideas for future research.

2. Related work

2.1. Deep learning in COVID-19 diagnosis

With the rise of deep learning methods in medical image processing, techniques have also been developed for COVID-19, normal, and CAP cases using X-rays and CT images [19,20]. Nwosu and his colleagues [21] proposed a two-channel residual neural network with a semi-supervised learning strategy to classify normal, pneumonia, and COVID-19 images via chest X-rays. Waheed et al. [22] developed a variant generative adversarial network (GAN), CovidGAN, to generate synthetic X-ray images for the classification of normal and COVID-19 cases. Ouyang et al. [23] integrated online attention with 3D ResNet-34 in developing a dual-sampling attention network for distinguishing COVID-19 from CAP. Nagi and his colleagues [20] utilized a

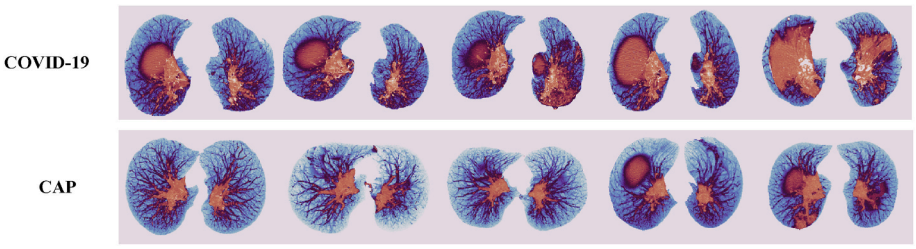

Fig. 2. Some examples of MIP images of COVID-19 and CAP.

custom deep learning model, namely a modified version of MobileNet-v2, and an extended Xception model for the classification of COVID-19, lung opacity, and normal X-ray images. The above methods employed conventional X-ray images, which do not provide a significant amount of detail in the lungs.

CT images provide a more detailed view of the lungs, soft tissue, and blood vessels [24]. Mohammed et al. [25] proposed an integrated method for selecting the optimal deep learning model based on a novel crow swarm optimization algorithm for COVID-19 diagnosis using CT images. Saeed et al. [26] proposed a method based on complex fuzzy hyper-soft sets, which is a formulation of complex fuzzy (CF) and hyper-soft sets for the classification of COVID-19 and non-COVID-19. Mahmoudi et al. [27] proposed a CNN-based method for detecting and quantifying COVID-19 using CT images, while another study utilized a modified U-Net for COVID-19 lung infection segmentation [28]. Ibrahim et al. [29] investigated hybrid deep learning methods that can quickly and accurately identify COVID-19 from non-COVID-19 using lung CT images. They developed a diagnosis system starting with the segmentation of lung CT scan images and ending with disease prediction, giving a reliable COVID-19 prediction method.

2.2. Capsule network in medical image classification

Capsule networks provide a novel approach to creating synthetic neurons. Several studies have demonstrated how widely capsule networks are used in several sectors [30], including image classification. Capsule networks have achieved state-of-the-art performance on datasets such as CIFAR-10 [31,32], Fashion MNIST [33], MNIST [34], and SVHN [35]. Different feature extractors can be employed with capsule networks, including DenseNet [36], ResNet [37], Res2Net and SE-Block [38], and ResNet-v2 [39]. Recently, capsule networks have been exploited for COVID-19 diagnosis [40,41]. Gupta et al. [42] proposed the COVID-WideNet for detecting COVID-19 from non-COVID-19 cases based on a capsule network with two convolutional layers and three capsule layers with less-trainable parameters. Li and his colleagues [43] proposed a novel capsule network with a non-iterative and parameterized multi-head attention routing algorithm to replace the traditional iterative dynamic routing process. This method extracts more generalized representation features from X-ray images, thus improving the classification of COVID-19, pneumonia, and normal cases.

3. Materials and methods

3.1. Dataset

Data were acquired from different hospitals and publicly available datasets. Table 1 summarizes these datasets. The details are as follows.

- The lab dataset contains 168 CT scans from 56 patients with COVID-19 and 165 scans from 100 patients with CAP. These images were taken between December 2019 and March 2020 at the General Hospital of the Yangtze River Shipping and Affiliated Hospital of Guizhou Medical University. RT-PCR tests were used to diagnose the COVID-19 patients.

Table 1
Summary of CT scans of COVID-19 and CAP in the datasets.

Dataset	Category		Total
	COVID-19	CAP	
Lab dataset	161/35	165/31	326
CC-CCII	1245	1471	2716
TCIA	629	–	629
Dongguan dataset	236	–	236

- The China Consortium of Chest CT Image Investigation (CC–CCII) dataset consists of 2716 CT scans (or patients), in which 1245 CT scans (or patients) were diagnosed with COVID-19 and 1471 CT scans (or patients) were diagnosed with CAP [44].
- The Cancer Imaging Archive (TCIA) dataset compromises 629 CT scans from 538 patients with COVID-19 [45].
- The Dongguan dataset consists of 236 CT scans from 158 patients with COVID-19. The dataset was obtained from Wanjiang People's Hospital. The patients were scanned by GE Medical Systems CT and Philips HOST-100196 CT.

3.2. Overview of the study procedure

Fig. 3 represents the overall workflow of the proposed method for distinguishing COVID-19 from CAP using MIP images generated by CT scans and a capsule network. First, 2D slices are extracted from CT scans for segmenting the lung mask. Segmentation methods including LinkNet, U-Net, Recurrent Residual CNN-based U-Net (R2U-Net), Attention U-Net, U-Net++, and CE-Net are applied to the 2D CT images. Second, MIP images are produced from the superposition of maximum gray in intrapulmonary CT values. Finally, the MIP images are input into the capsule network for patient-level prediction of the final COVID-19 diagnosis. The feature extractors of the capsule network consist of ResNet-50, Inception-V3, and DenseNet-121. Details of each step of the proposed method are described in the following sections.

3.3. Lung segmentation

As the CT scans were acquired from different CT scanners and hospitals, a fixed window (window level = −300 HU, window width = 1400 HU) was set and the CT images were normalized to the range [0, 1]. The lung masks for 161 CT scans of COVID-19 were annotated in a semi-automatic way. First, the Pulmonary Toolkit (https://github.com/tomdoel/pulmonarytoolkit) was employed to initially segment the mask of the lung field. The mask was then manually modified by radiologists. The preprocessed CT images and annotations of the lung mask were fed into the segmentation model for training and evaluation. LinkNet [46] was used to segment the lung parenchyma. The network architecture is depicted in Fig. 4. Similar to U-Net [47], LinkNet is composed of an encoder and a decoder, which are interconnected by an addition operation. In the encoder part, LinkNet uses ResNet-34 [48] pretrained on the ImageNet dataset [49], with the fully connected layer and the global average pooling layer removed. The decoder has five blocks, each consisting of a 2×2 up-sampling layer followed by two sets of layers, each

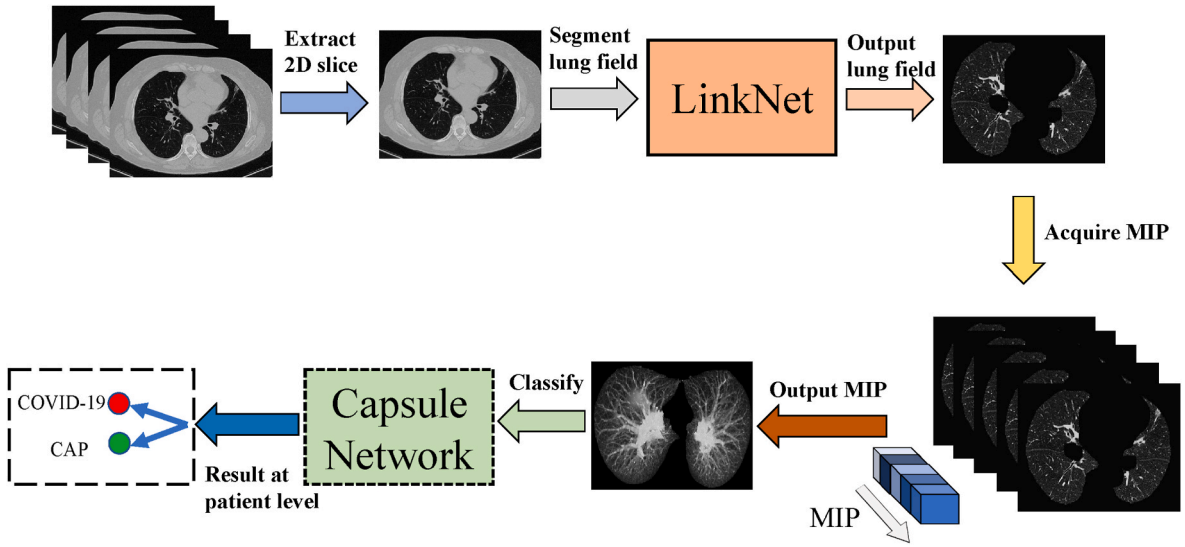

Fig. 3. Workflow of the proposed method for distinguishing COVID-19 and CAP.

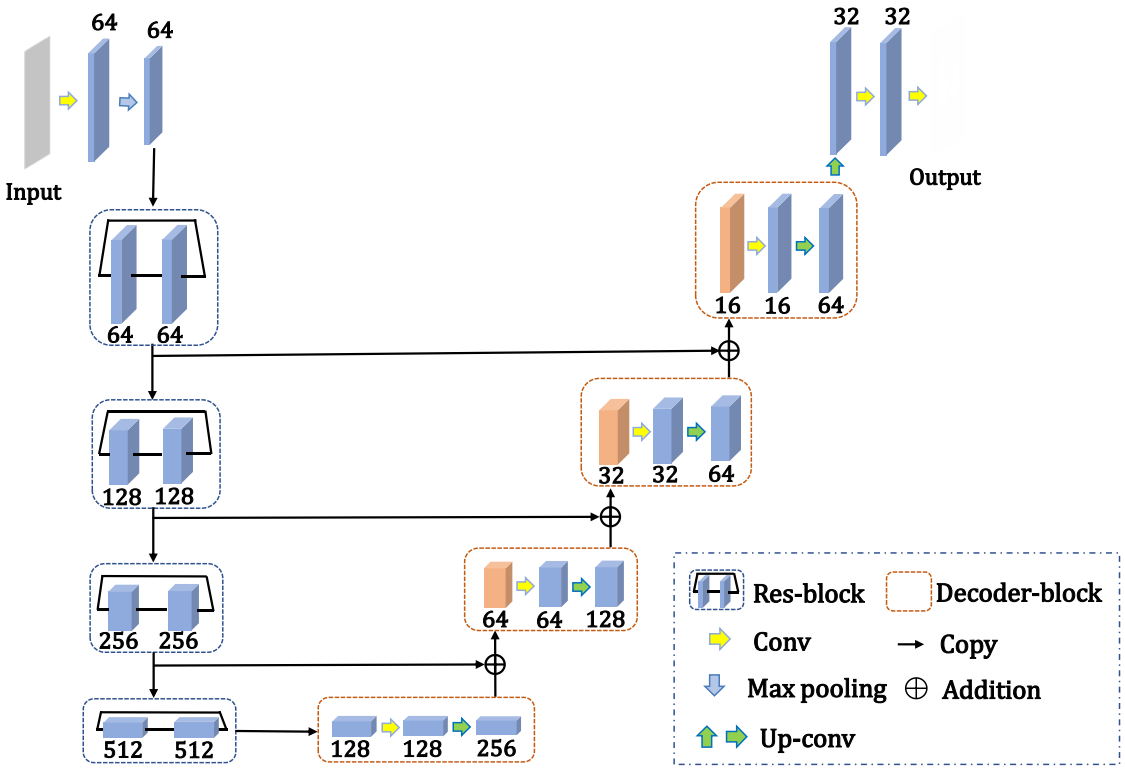

Fig. 4. Architecture of LinkNet for lung segmentation.

containing a convolution layer, batch normalization layer, and rectified linear unit (ReLU) activation layer. In the first four blocks of the decoder, feature maps are generated from the corresponding part in the encoder and added to the feature map after up-sampling. Finally, a 3×3 convolution layer followed by sigmoid activation is applied to output the binary masks of the lung field.

The binary cross-entropy (BCE) was applied as the loss function in the segmentation network. This function is expressed as follows:

$$Loss_{BCE} = -\frac{1}{n}\Sigma(y_n \ln x_n + (1 - y_n)(1 - \ln x_n)) \# (1)$$

where x_n represents the prediction of the network and y_n represents the ground-truth (annotated lung mask).

The morphological filling method, namely the "Find Contours" function in the OpenCV library, was applied to enhance the performance of lung mask segmentation. Five existing segmentation networks, i.e., U-Net [47], R2U-Net [50], Attention U-Net [51], U-Net++ [52,53], and CE-Net, were compared with our lung segmentation model.

3.4. Acquisition of MIP images

In clinical practice, radiologists usually examine axial sections of

patients' CT images to differentiate between COVID-19 lesions and CAP. Moreover, MIP images are routinely used by radiologists to improve the detection of COVID-19. In our method, MIP images are acquired through the superposition of maximum CT values at each coordinate from a stack of consecutive slices.

3.5. MIP-based capsule network for prediction of COVID-19 and CAP

As shown in Fig. 5, using an MIP image as input, the capsule network was trained for the patient-level prediction of COVID-19 and CAP. The capsule network consists of a feature extraction module (DenseNet-121 backbone) and a capsule module including a primary capsule, convolutional capsules A and B, and a dense capsule.

The input image measures 512 × 512 pixels. The first three stages of the pretrained DenseNet-121 [48] are used as a feature extraction block. As shown in Fig. 6, the feature extraction block is comprised of a convolutional layer with 7 × 7 filters, a max pooling layer, four dense blocks, three transition layers, and a global average pooling layer. The dense block consists of different numbers of conv_block units, which perform batch normalization, ReLU activation, and convolution with 1 × 1 and 3 × 3 filters. A transition layer is placed between adjacent dense blocks. Finally, 1024 features are output from the DenseNet-121 block and transmitted to the primary capsule layer.

Each capsule module consists of a primary capsule layer and two convolution capsule layers. The primary capsule layer is preceded by a convolutional layer (512 kernels of size 1 × 1), which processes the output features of DenseNet-121. Dynamic routing is followed by the primary capsule layer, which is used to reshape the output of the former convolutional block.

The probability of two categories is obtained by the dense capsule layer. The norm of the two capsules (i.e., the output of the capsule network) is input into a SoftMax operation to produce the final prediction.

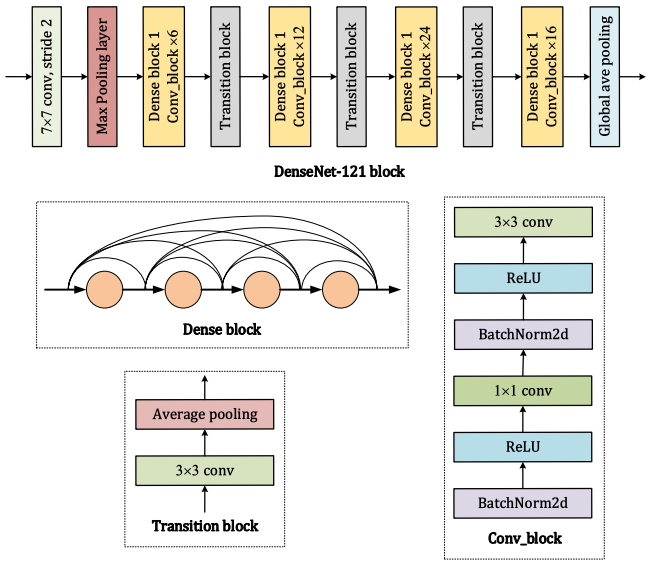

Fig. 6. Architecture of DenseNet-121 in the capsule network.

A spread loss function reduces the sensitivity of training to the model initialization and super-parameters. The following spread loss function was used to train the network:

$$Loss_{Spread} = \Sigma_{t \neq i}\, max(0, m - (a_t - a_i))^2 \#(2)$$

where a_t and a_i represent the activation values of the target and the i-th position from the target, respectively.

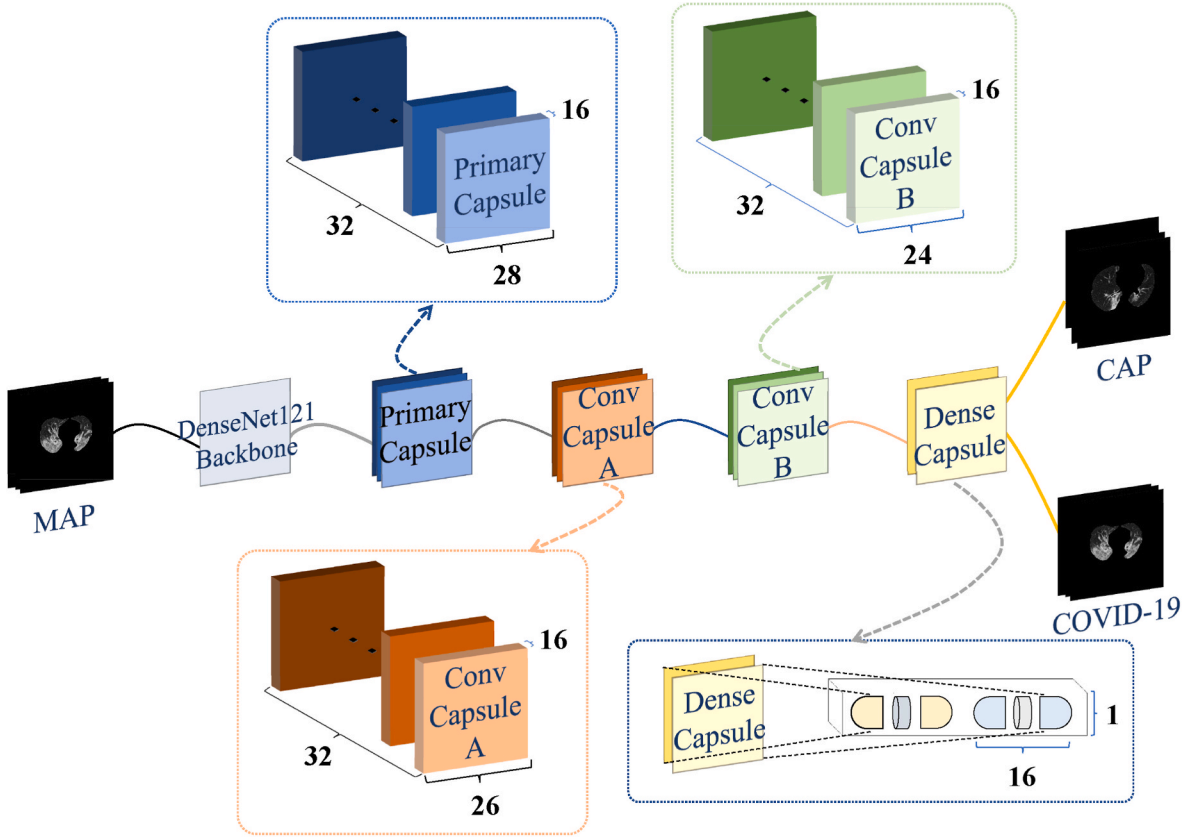

Fig. 5. Architecture of the capsule network for the prediction of COVID-19 and CAP.

3.6. Ablation experiments

Three comparative experiments were conducted. The first attempted to determine whether the segmentation of the lung field improves the performance of distinguishing COVID-19 from CAP. For this, the MIP images generated by the original CT images without lung segmentation and the intrapulmonary CT images were input to the capsule network for prediction.

The second experiment attempted to determine whether the MIP images are useful. Following our previous study [13], all intrapulmonary slices were directly fed into the capsule network and the slice-level predictions were output. Majority voting was then utilized to produce the final patient predictions.

The third experiment examined whether the capsule network affects the classification performance of COVID-19 and CAP. In this experiment, the capsule modules were replaced by the vanilla DenseNet-121 blocks.

3.7. Experimental setup

During the experiments on the lung segmentation network, we marked the lung fields on 161 CT scans, including 10,280 image slices of COVID-19. The dataset was divided into training, validation, and testing sets at a ratio of 7:1:2. To train the capsule network on our lab dataset, 333 MIP images generated from 333 CT scans were divided into training, validation, and testing sets at a ratio of 8:1:1. The CC-CCII, TCIA, and Dongguan datasets were used as external independent datasets for testing. Data augmentation was implemented in the training stage via scaling and random rotation in the horizontal and vertical directions. Early stopping was adopted to alleviate the problem of overfitting when the validation accuracy did not increase over five epochs.

For the segmentation task, the batch size was set to 8, the initial learning rate was 1×10^{-4}, the Adam optimizer was used, and the number of epochs was fixed to 50. For the classification task, the batch size was set to 16, the number of epochs was 25, the initial learning rate was 1×10^{-4}, the Adam optimizer was used, and the number of dynamic routing iterations of the capsule network was set to 3. The experiments were implemented using PyTorch as a deep learning framework. The models were trained on a workstation with an Intel Core I7-9700 3.00 GHz CPU and four NVIDIA GeForce RTX 2080 Ti GPUs.

3.8. Evaluation metrics

The intersection over union (IoU) and Dice coefficient were used to evaluate the lung segmentation performance. The accuracy, precision, sensitivity, specificity, and area under the curve (AUC) were used to evaluate the classification models.

$$\text{IoU} = \frac{TP}{TP + FN + FP} \#(3)$$

$$\text{Dice} = \frac{2TP}{2TP + FN + FP} \#(4)$$

$$\text{Accuracy} = \frac{\text{TP} + \text{TN}}{\text{TP} + \text{TN} + \text{FP} + \text{FN}} \#(5)$$

$$\text{Precision} = \frac{TP}{TP + FP} \#(6)$$

$$\text{Sensitivity} = \frac{TP}{TP + FN} \#(7)$$

$$\text{Specificity} = \frac{TN}{FP + TN} \#(8)$$

For the IoU and Dice metrics, TP is the number of true positives and FN is the number of false negatives. In the classification metrics, TP indicates the number of COVID-19 patients correctly classified as COVID-19 patients by the proposed model, FP (false positive) denotes the number of CAP patients falsely classified as COVID-19 patients, FN denotes the number of COVID-19 patients falsely classified as CAP patients, and TN (true negative) indicates the number of CAP patients correctly classified as CAP patients.

4. Results

4.1. Lung segmentation

The lung segmentation performance using the six different models is summarized in Table 2. LinkNet achieves the best performance, with IoU and Dice coefficient scores of 0.967 and 0.983. This confirms that LinkNet is beneficial for lung segmentation. Conversely, R2U-Net gives the minimum IoU (0.928) and Dice coefficient (0.962).

Some examples of the lung segmentation results extracted from COVID-19 CT images are depicted in Fig. 7. Under-segmented regions can be observed in the results given by U-Net, R2U-Net, Attention U-Net, U-Net++, and CE-Net. Overall, parts of the CT scanner bed are incorrectly detected and segmented as lung field regions.

4.2. Prediction of capsule network using three different backbones on lab dataset

Fig. 8 shows the confusion matrix of the capsule network on the lab dataset with different feature extraction modules (ResNet-50, Inception-V3, and DenseNet-121). This shows which CNN feature extractor achieves the best classification accuracy. The testing dataset contains 66 MIP images, 35 for COVID-19 and 31 for CAP. The ResNet-50, Inception-V3, and DenseNet-121 modules correctly identified 27, 28, and 34 COVID-19 patients and 29, 29, and 30 CAP patients, respectively.

The number of parameters, accuracy, precision, sensitivity, and specificity scores using the ResNet-50, Inception-V3, and DenseNet-121 modules are reported in Table 3. The capsule network using DenseNet-121 achieves the best performance in classifying COVID-19 and CAP with the fewest training parameters (accuracy of 97.0%, precision of 0.971, sensitivity of 0.971, specificity of 0.968, and AUC of 0.986; see Fig. 9). In second place, Inception-V3 uses the most training parameters to achieve 86.4% accuracy and 0.883 AUC. The ResNet-50 backbone gives the minimum accuracy (84.9%), precision (0.931), sensitivity (0.771), and specificity (0.935). We can see that the capsule network with the DenseNet-121 backbone produces the best overall performance on the COVID-19 and CAP categories.

4.3. Predictions for other datasets

Fig. 10 and Table 4 summarize the performance of the capsule network on the CC-CCII, TCIA, and Dongguan datasets. The experiments confirm the capsule network is beneficial and robust for COVID-19 diagnosis. The CC-CCII dataset consists of COVID-19 and CAP cases. As shown in Fig. 9(a), for the COVID-19 category, 187 of 201 items are correctly predicted, while for the CAP category, the proposed method correctly classifies 261 of 265 items. Moreover, the accuracy, precision, sensitivity, specificity, and AUC in terms of distinguishing the two categories are 0.961, 0.979, 0.930, 0.985, and 0.971, respectively. The

Table 2
Performance of the six lung segmentation networks.

Model	IoU	Dice
U-Net [54]	0.962	0.980
LinkNet	**0.967**	**0.983**
R2U-Net [50]	0.928	0.962
Attention U-Net	0.951	0.974
U-Net++ [52,53]	0.936	0.966
CE-Net	0.964	0.981

* Bold font indicates the network with the best performance.

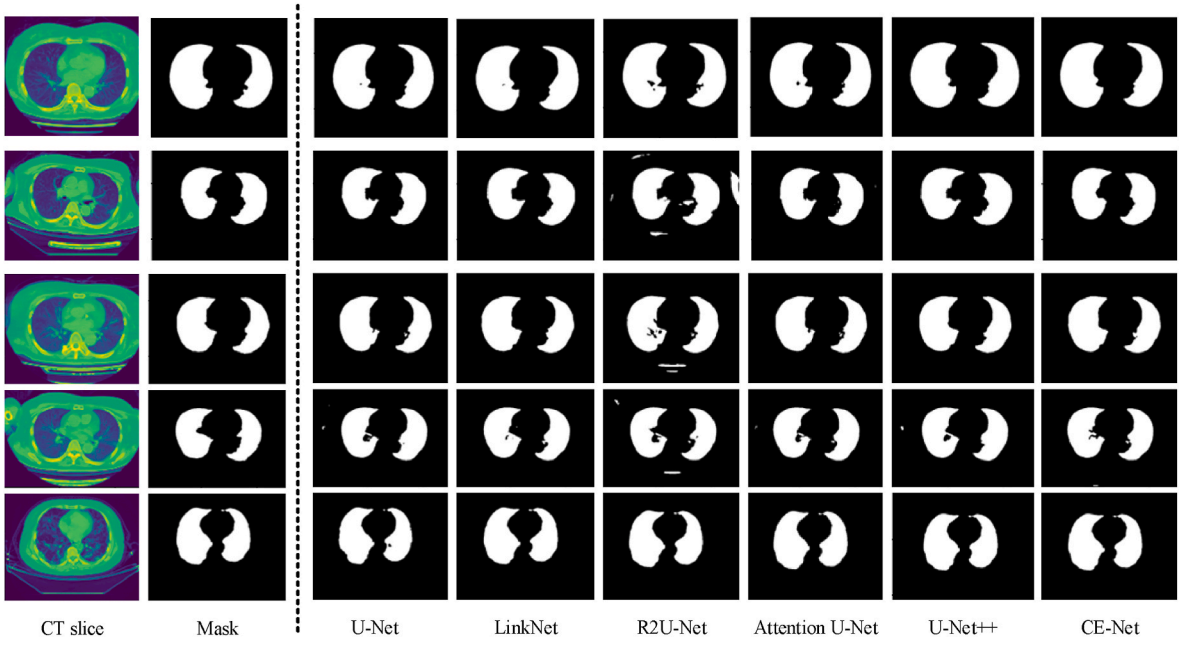

Fig. 7. Examples of lung segmentation using different networks.

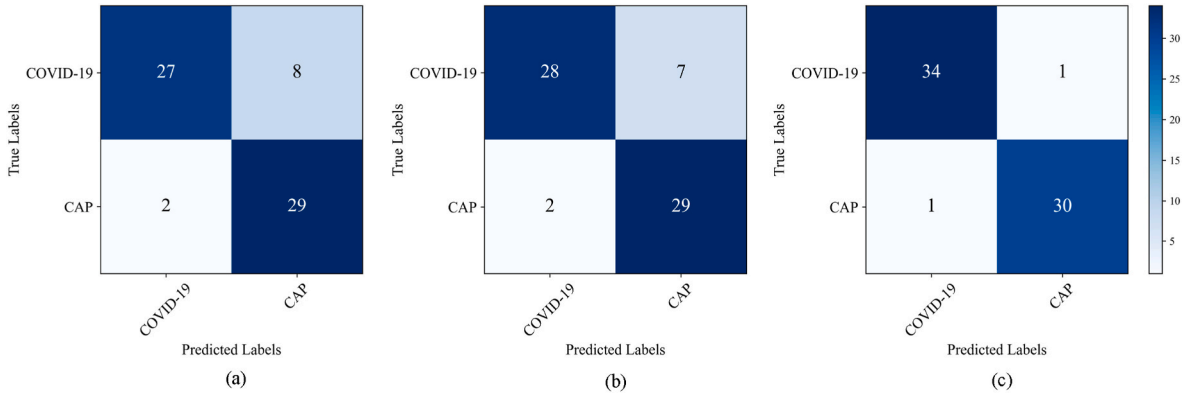

Fig. 8. Confusion matrix for the classification of COVID-19 and CAP using three different feature extraction modules. (a) ResNet-50; (b) Inception-V3; (c) DenseNet-121.

Table 3
Performance comparison of different feature extraction modules using capsule network.

Model	Params. (M)	Accuracy	Precision	Sensitivity	Specificity	AUC
ResNet-50	9.63	0.849	0.931	0.771	0.935	0.910
Inception-V3	9.92	0.864	0.933	0.800	0.935	0.883
DenseNet-121	**8.04**	**0.970**	**0.971**	**0.971**	**0.968**	**0.986**

* Bold font indicates the best value among the three models.

TCIA and Dongguan datasets only consist of COVID-19 patients. As shown in Fig. 10(b) and (c), the number of correctly predicted COVID-19 cases is 627 out of 629 and 224 out of 236 cases. The accuracy of COVID-19 diagnosis with the TCIA and Dongguan datasets is 99.7% and 94.9%, respectively. In this case, we conclude that the proposed method is beneficial and robust for the diagnosis of COVID-19 on multiple datasets.

4.4. Results of the ablation experiment

Ablation experiments were conducted to analyze the proposed method's key components. As shown in Table 5, the main components are the lung segmentation, MIP image generation, and capsule network. Without applying lung segmentation before the acquisition of MIP images, the accuracy decreases to 63.5%. In this situation, the MIP images are directly generated by the CT scan and may include redundant information, such as the patient table and bone information. If we use the raw CT images rather than the MIP images (i.e., the patient-level prediction is produced by majority voting on the predictions of the capsule network via each slice of the CT images), the accuracy is only 85.7%, approximately 11.3% lower than when using the MIP images. Removing the capsule network and only using the DenseNet-121 network for classification reduces the accuracy to 81.8%. Thus, we conclude that lung segmentation, MIP images, and the capsule network are all

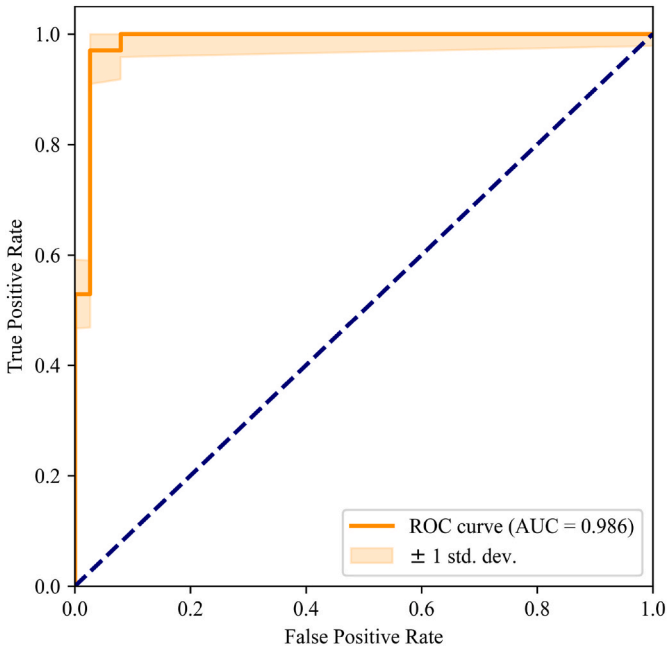

Fig. 9. ROC curve of the capsule network with DenseNet-121.

beneficial to distinguishing COVID-19 from CAP using CT images. The three components of the proposed method help boost the classification performance.

4.5. Comparison of our method with current state-of-the-art techniques

We investigated other state-of-the-art methods for classifying COVID-19 and compared them with our proposed method. The results in Table 6 show that our proposed method achieves an accuracy of 0.970, outperforming all state-of-the-art methods except for our previous approach. The sensitivity of our method is higher than or comparable to that of the pipeline mimicking radiologist [13], a combination of CNN and SVM [55], multi-instance learning and a long short-term memory (LSTM) network [56], weakly supervised multi-scale learning [4], $M_{ResNet-50-MIL}$ [12], a 2D CNN [57], a semi-supervised learning strategy with multi-view fusion [58], the BigBiGAN framework [59], the pre-trained EfficientNet-b7 [60], and 3D ResNet-34 with attention modules [23].

4.6. Interpretation of our method using t-SNE

As described in Fig. 11, the full complexity of distinguishing COVID-19 from CAP can be illustrated by visualizing the parameter space of patients with COVID-19 and CAP from our lab testing data using the t-distributed stochastic neighbor embedding (t-SNE) method [62]. Although COVID-19 and CAP produce highly similar CT images, the predictions of our proposed capsule network using three different backbones have a significant non-overlap. The medoid of the COVID-19 group lies farther away from that of the CAP group in Fig. 10(c) than in Fig. 10(a) and (b). As expected, this demonstrates that our proposed method with the DenseNet-121 backbone has an extremely high discriminative power between COVID-19 and CAP.

5. Discussion

5.1. Challenges in lung segmentation and distinguishing COVID-19 from CAP using CT images

Lung segmentation is a crucial preprocessing step for the classification network. It reduces the impact of tissues outside the lung field and enables the capsule network to focus on the lesions within the lung field. Moreover, the intrapulmonary parenchyma is the prerequisite for the generation of MIP images. However, segmenting the lung field in COVID-19 and CAP patients is challenging due to the impact of lesions in CT images. Six off-the-shelf CNN models (U-Net, LinkNet, R2U-Net, Attention U-Net, U-Net++, and CE-Net) were employed for lung segmentation. LinkNet outperformed the other five networks, achieving a Dice coefficient of 0.983 and an IoU of 0.967. These scores are greater than or comparable to previous results obtained using DenseNet-161 U-Net [63], Lung Seg-Net [64], and three-stage segmentation [65].

CT is one of the most widely used imaging methods in clinical practice [66–69] and plays an important role in the diagnosis of CAP and epidemiological studies [70]. Ground-glass opacities, consolidation, and peripheral and bilateral involvement have been observed in CT images of COVID-19 [71]. However, in CT images, COVID-19 exhibits many

Table 4
Performance comparison on different datasets.

Dataset	Accuracy	Precision	Sensitivity	Specificity	AUC
CC-CCII	0.961	0.979	0.930	0.985	0.971
TCIA	0.997	–	–	–	–
Dongguan	0.949	–	–	–	–

Table 5
Performance comparison with different pretraining blocks.

Ablation experiment	Accuracy
Lung segmentation (−)	63.5%
MIP (−)	85.7%
Capsule networks (−)	81.8%
Our method	**97.0%**

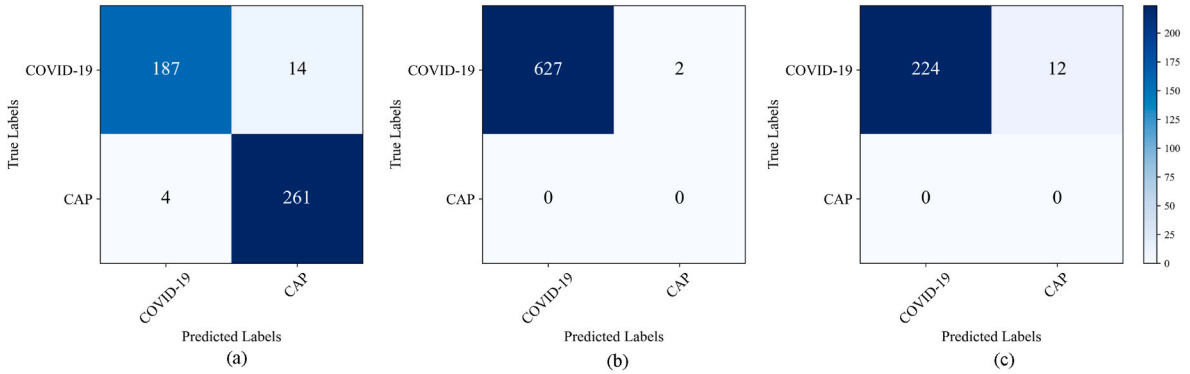

Fig. 10. Confusion matrix on other datasets. (a) CC-CCII dataset; (b) TCIA dataset; (c) Dongguan dataset.

Table 6
Performance of our method against state-of-the-art methods.

Ref	Dataset	Method	Performance			
			Acc.	Sen.	Spe.	AUC
Our proposed method	156 patients (56 COVID-19 and 100 CAP)	- Lung segmentation - MIP	0.970	0.971	0.968	0.986
HU et al., 2022 [4]	450 patient scans (150 of COVID-19, CAP and NP)	- Lung segmentation - Weakly supervised multi-scale learning	0.891	0.870	0.862	0.906
Qi et al., 2022 [13]	157 patients (57 COVID-19 and 100 CAP)	- Lung segmentation - Selection of slices with lesions - Slice-level prediction - Patient-level prediction	0.971	0.959	0.981	0.992
Ibrahim et al., 2022 [29]	2984 patients (COVID-19: 1396; non-COVID-19: 1588)	- VGGNet - Convolutional deep belief network - High-resolution network	0.95	0.95	0.96	
Erdal et al., 2022 [55]	2496 CT scans (1428 COVID-19 and 1068 CAP)	- Deep CNN for feature extraction - SVM classification	0.932	0.858	0.993	0.984
Xu et al., 2022 [56]	515 patients (204 COVID-19 and 311 CAP)	- Multi-instance learning - LSTM	–	0.862	0.980	0.956
Li et al., 2022 [61]	4352 CT scans (1292 COVID-19, 1735 CAP, and 1325 non-pneumonia)	- Lung segmentation - 2D local and 3D global representative features	–	0.885	0.940	0.955
Zhu et al., 2022 [58]	2522 patients (1495 COVID-19 and 1027 CAP)	- Semi-supervised strategy - Multi-view fusion method - Pairwise constraint regularization	0.920	0.931	0.904	0.963
Qi et al., 2021 [12]	241 patients (COVID-19: 141; CAP: 100)	- Multi-instance learning - Deep features extracted by ResNet-50	0.959	0.972	0.941	0.955
Javaheri et al., 2021 [57]	335 CT scans (111 COVID-19, 115 CAP, 109 Normal)	- Training a subset of the control dataset model - Feeding all the datasets into the trained model	0.933	0.909	1.00	0.940
Basset et al., 2021 [60]	305 CT scans (169 COVID-19; 60 CA; 76 Normal)	- Lung segmentation - EfficientNet-b7 for features - Attention modules learn multi-scale features	0.968	–	–	0.988
Ouyang et al., 2020 [23]	- 3645 CT images (COVID-19: 2565; CAP: 1080)	- Lung segmentation - 3D ResNet-34 - Attention module and ensemble learning	0.875	0.869	0.901	0.944
Song et al., 2020 [59]	201 CT images (COVID-19: 98; non-COVID-19: 103)	- BigBiGAN framework - Linear classifier	–	0.920	0.910	0.972

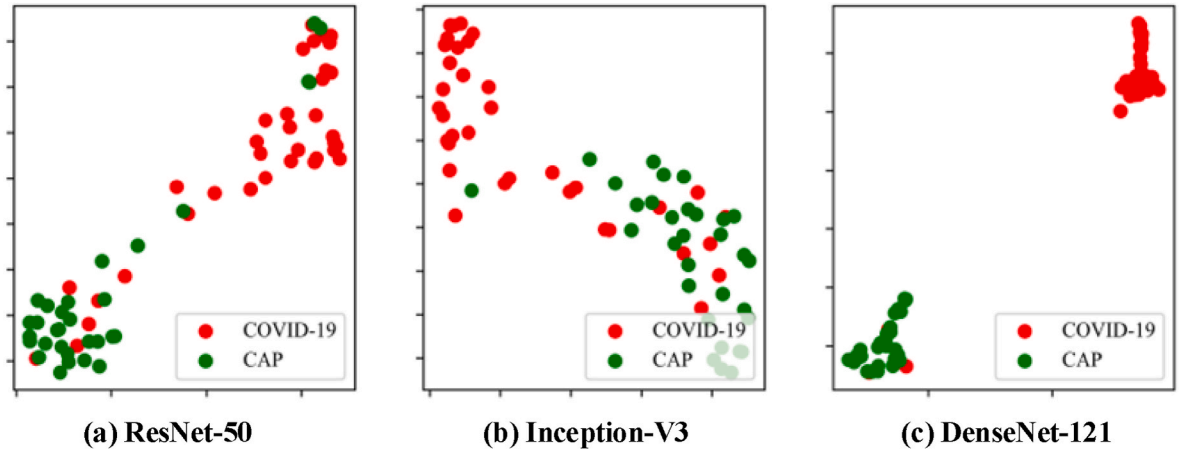

Fig. 11. Visualization of COVID-19/CAP parameter space with the t-SNE method using a capsule network with different backbones. Each dot represents a patient and its color represents the group. Red dots represent patients with COVID-19 and green dots represent patients with CAP. (a) ResNet-50; (b) Inception-V3; (c) DenseNet-121.

similarities to CAP, i.e., high similarity to pneumonia of different types (especially in the early stage) and large variations in different stages of the same type [72,73]. Hence, it is vital to develop an automatic deep learning-based diagnosis algorithm specific to COVID-19. In our previous studies [12,13], the automatic pipeline mimicking radiologist and multiple-instance learning (MIL) methods were developed for distinguishing COVID-19 from CAP. These methods achieved accuracy scores of 97% and 95% and AUC scores of 0.992 and 0.955, respectively. Our proposed method outperformed the MIL method and produced comparable results to the automatic pipeline [13]. This is also evident from our t-SNE analysis and visualization of the distribution of COVID-19 and CAP cases in Fig. 10, which illustrate the complexity of the parameter space.

5.2. Advantages of MIP images

In this work, the MIP method was developed to consider the routine workflow of radiologists. In clinical practice, radiologists quickly scan the MIP images to determine the pneumonia candidates for additional investigations on specific slices. Postprocessing through MIP [17] transfers 3D voxels to the plane of projection at their highest intensity. As this improves the visibility of nodules in comparison to the presence of bronchi and vasculature, it is frequently utilized for the identification of lung nodules [74]. Inspired by this initial procedure, we proposed an MIP-based capsule network approach. The results presented herein demonstrate that the combination of MIP and CNN improves the accuracy and efficiency of COVID-19 classification.

5.3. Limitations and further studies

The proposed approach still has certain limitations. First, the size of the dataset is small, and so a more diverse population from more centers is required to verify the performance of the proposed method. Second, gathering more subjects exhibiting other pneumonia subtypes, lung diseases, and even healthy individuals would help improve the diagnosis ability. Third, building a larger dataset with linked CT and clinical data, especially data on underlying disorders, would allow for further research of the diagnosis system and the development of further functionality, including assessments of the severity of the disease. Fourth, the current method only focuses on the analysis of the lung parenchyma in CT images. Some segmentation methods of lung airways and vessels have been established using deep learning-based methods. The analysis of airways and vessels in COVID-19 patients using CT images could be considered. Finally, more advanced methods, such as GANs [75] and ensemble learning [76], could improve the diagnosis performance of COVID-19.

6. Conclusion

This work proposed a novel method of distinguishing COVID-19 from CAP using MIP images from CT scans and a capsule network. The performance of the method demonstrates the significance and effectiveness of MIP images for COVID-19 detection in CT scans. This study has demonstrated that MIP images provide conspicuous benefits when exploiting CNNs to detect COVID-19 lesions.

To the best of our knowledge, there is a high degree of similarity between COVID-19 and CAP in chest CT images. This increases the need for a diagnosis system that distinguishes COVID-19 from CAP in CT images. The proposed method combines the advantages of MIP images and capsule networks to address this issue. This system could reduce radiologists' workloads by significantly decreasing the number of scans that need to be manually evaluated. This work provides a new direction for the usage of CT scans in COVID-19 diagnosis.

The main limitation of the present study is the small set of training data. Although data were obtained from multiple centers, the overall size of the data is relatively small. Gathering more subjects exhibiting other pneumonia subtypes would help improve the range of diagnosis. Moreover, assessments of the severity of COVID-19 should be included in further research on the diagnosis system. The proposed diagnosis system can be extended to other diseases and other modalities, such as the transfer learning of the approach for lung cancer classification.

Ethical approval

All procedures performed in studies involving human participants were in accordance with the ethical standards of the institutional and/or national research committee and with the 1964 Helsinki declaration and its later amendments or comparable ethical standards.

Informed consent

Informed consent was waived because this was a prospective study.

Declaration of competing interest

The authors declare that they have no known competing financial interests or personal relationships that could have appeared to influence the work reported in this paper.

Acknowledgments

Funding: This work was supported by the National Natural Science Foundation of China [grant numbers 82072008, 82270044]; the Fundamental Research Funds for the Central Universities [grant numbers N2119010, N2124006-3]; and the Foshan Special Project of Emergency Science and Technology Response to COVID-19 [grant number 2020001000376].

References

[1] M.M. Rahaman, C. Li, Y. Yao, F. Kulwa, M.A. Rahman, Q. Wang, S. Qi, F. Kong, X. Zhu, X. Zhao, Identification of COVID-19 samples from chest X-Ray images using deep learning: a comparison of transfer learning approaches, J. X Ray Sci. Technol. 28 (5) (2020) 821–839.
[2] P. Mehta, D.F. McAuley, M. Brown, E. Sanchez, R.S. Tattersall, J.J. Manson, COVID-19: consider cytokine storm syndromes and immunosuppression, Lancet 395 (10229) (2020) 1033–1034.
[3] V.M. Corman, O. Landt, M. Kaiser, R. Molenkamp, A. Meijer, D.K. Chu, T. Bleicker, S. Brünink, J. Schneider, M.L. Schmidt, Detection of 2019 novel coronavirus (2019-nCoV) by real-time RT-PCR, Euro Surveill. 25 (3) (2020), 2000045.
[4] S. Hu, Y. Gao, Z. Niu, Y. Jiang, L. Li, X. Xiao, M. Wang, E.F. Fang, W. Menpes-Smith, J. Xia, Weakly supervised deep learning for covid-19 infection detection and classification from CT images, IEEE Access 8 (2020) 118869–118883.
[5] M. Farooq, A. Hafeez, Covid-resnet: A Deep Learning Framework for Screening of Covid19 from Radiographs, 2020 *arXiv preprint* arXiv:2003.14395.
[6] J. Li, G. Zhao, Y. Tao, P. Zhai, H. Chen, H. He, T. Cai, Multi-task contrastive learning for automatic CT and X-ray diagnosis of COVID-19, Pattern Recogn. 114 (2021), 107848.
[7] H. Meng, R. Xiong, R. He, W. Lin, B. Hao, L. Zhang, Z. Lu, X. Shen, T. Fan, W. Jiang, CT imaging and clinical course of asymptomatic cases with COVID-19 pneumonia at admission in Wuhan, China, J. Infect. 81 (1) (2020) e33–e39.
[8] A.A. Ardakani, R.M. Kwee, M. Mirza-Aghazadeh-Attari, H.M. Castro, T.Y. Kuzan, K. M. Altintoprak, G. Besutti, F. Monelli, F. Faeghi, U.R. Acharya, A practical artificial intelligence system to diagnose COVID-19 using computed tomography: a multinational external validation study, Pattern Recogn. Lett. 152 (2021) 42–49.
[9] A. Gulati, LungAI: A Deep Learning Convolutional Neural Network for Automated Detection of COVID-19 from Posteroanterior Chest X-Rays, MedRxiv, 2020.
[10] D. Haritha, M.K. Pranathi, M. Reethika, COVID detection from chest X-rays with DeepLearning: CheXNet, in: 2020 5th International Conference on Computing, Communication and Security (ICCCS), IEEE, 2020, pp. 1–5.
[11] O. Gozes, M. Frid-Adar, H. Greenspan, P.D. Browning, H. Zhang, W. Ji, A. Bernheim, E. Siegel, Rapid AI Development Cycle for the Coronavirus (Covid-19) Pandemic: Initial Results for Automated Detection & Patient Monitoring Using Deep Learning CT Image Analysis, 2020 *arXiv preprint arXiv*:2003.05037.
[12] S. Qi, C. Xu, C. Li, B. Tian, S. Xia, J. Ren, L. Yang, H. Wang, H. Yu, DR-MIL: deep represented multiple instance learning distinguishes COVID-19 from community-acquired pneumonia in CT images, Comput. Methods Progr. Biomed. 211 (2021), 106406.
[13] Q. Qi, S. Qi, Y. Wu, C. Li, B. Tian, S. Xia, J. Ren, L. Yang, H. Wang, H. Yu, Fully automatic pipeline of convolutional neural networks and capsule networks to distinguish COVID-19 from community-acquired pneumonia via CT images, Comput. Biol. Med. 141 (2022), 105182.
[14] D.C. Rotzinger, S.D. Qanadli, Should vascular abnormalities Be integrated into the chest CT imaging signature of coronavirus disease 2019? Chest 159 (5) (2021) 2107–2108.
[15] J. Poletti, M. Bach, S. Yang, R. Sexauer, B. Stieltjes, D.C. Rotzinger, J. Bremerich, A. W. Sauter, T. Weikert, Automated lung vessel segmentation reveals blood vessel volume redistribution in viral pneumonia, Eur. J. Radiol. 150 (2022), 110259.
[16] M. Lins, J. Vandevenne, M. Thillai, B.R. Lavon, M. Lanclus, S. Bonte, R. Godon, I. Kendall, J. De Backer, W. De Backer, Assessment of small pulmonary blood vessels in COVID-19 patients using HRCT, Acad. Radiol. 27 (10) (2020) 1449–1455.
[17] M. Prokop, H.O. Shin, A. Schanz, C.M. Schaefer-Prokop, Use of maximum intensity projections in CT angiography: a basic review, Radiographics 17 (2) (1997) 433–451.
[18] S. Zheng, J. Guo, X. Cui, R.N. Veldhuis, M. Oudkerk, P.M. Van Ooijen, Automatic pulmonary nodule detection in CT scans using convolutional neural networks based on maximum intensity projection, IEEE Trans. Med. Imag. 39 (3) (2019) 797–805.

[19] K.H. Abdulkareem, S.A. Mostafa, Z.N. Al-Qudsy, M.A. Mohammed, A.S. Al-Waisy, S. Kadry, J. Lee, Y. Nam, Automated system for identifying COVID-19 infections in computed tomography images using deep learning models, J. Healthc. Eng. 2022 (2022), 5329014.
[20] A.T. Nagi, M.J. Awan, M.A. Mohammed, A. Mahmoud, A. Majumdar, O. Thinnukool, Performance Analysis for COVID-19 Diagnosis using custom and state-of-the-art deep learning models, Appl. Sci. 12 (13) (2022) 6364.
[21] L. Nwosu, X. Li, L. Qian, S. Kim, X. Dong, Semi-supervised Learning for COVID-19 Image Classification via ResNet, 2021 *arXiv preprint arXiv:2103.06140*.
[22] A. Waheed, M. Goyal, D. Gupta, et al., Covidgan: data augmentation using auxiliary classifier gan for improved covid-19 detection[J], IEEE Access 8 (2021) 91916–91923.
[23] X. Ouyang, J. Huo, L. Xia, F. Shan, J. Liu, Z. Mo, F. Yan, Z. Ding, Q. Yang, B. Song, Dual-sampling attention network for diagnosis of COVID-19 from community acquired pneumonia, IEEE Trans. Med. Imag. 39 (8) (2020) 2595–2605.
[24] Z. Ye, Y. Zhang, Y. Wang, Z. Huang, B. Song, Chest CT manifestations of new coronavirus disease 2019 (COVID-19): a pictorial review, Eur. Radiol. 30 (8) (2020) 4381–4389.
[25] M.A. Mohammed, B. Al-Khateeb, M. Yousif, S.A. Mostafa, S. Kadry, K. H. Abdulkareem, B. Garcia-Zapirain, Novel crow swarm optimization algorithm and selection approach for optimal deep learning COVID-19 diagnostic model, Comput. Intell. Neurosci. 2022 (2022), 1307944.
[26] M. Saeed, M. Ahsan, M.H. Saeed, A.U. Rahman, A. Mehmood, M.A. Mohammed, M. M. Jaber, R. Damaševičius, An optimized decision support model for COVID-19 diagnostics based on complex fuzzy hypersoft mapping, Mathematics 10 (14) (2022) 2472.
[27] R. Mahmoudi, N. Benameur, R. Mabrouk, M.A. Mohammed, B. Garcia-Zapirain, M. H. Bedoui, A deep learning-based diagnosis system for COVID-19 detection and pneumonia screening using CT imaging, Appl. Sci. 12 (10) (2022) 4825.
[28] S. Shamim, M.J. Awan, A. Mohd Zain, U. Naseem, M.A. Mohammed, B. Garcia-Zapirain, Automatic COVID-19 lung infection segmentation through modified unet model, J. Healthc. Eng. 2022 (2022), 6566982.
[29] D.A. Ibrahim, D.A. Zebari, H.J. Mohammed, M.A. Mohammed, Effective hybrid deep learning model for COVID-19 patterns identification using CT images, Expet Syst. (2022), e13010.
[30] S. Pawan, J. Rajan, Capsule Networks for Image Classification: A Review, Neurocomputing 509 (2022) 102–120.
[31] A. Fuchs, F. Pernkopf, Wasserstein Routed Capsule Networks, 2020 *arXiv preprint arXiv:*2007.11465.
[32] L. Zhao, X. Wang, L. Huang, An Efficient Agreement Mechanism in CapsNets by Pairwise Product, 2020 *arXiv preprint arXiv:*2004.00272.
[33] J. Gu, Interpretable graph capsule networks for object recognition, Proc. AAAI Conf. Artif. Intell. 35 (2) (2021) 1469–1477.
[34] J.E. Lenssen, M. Fey, P. Libuschewski, Group equivariant capsule networks, Adv. Neural Inf. Process. Syst. 31 (2018).
[35] S. Sabour, N. Frosst, G.E. Hinton, Dynamic routing between capsules, Adv. Neural Inf. Process. Syst. 30 (2017).
[36] S.S.R. Phaye, A. Sikka, A. Dhall, D.R. Bathula, Multi-level dense capsule networks, in: Asian Conference on Computer Vision, Springer, 2018, pp. 577–592.
[37] B. Jia, Q. Huang, DE-CapsNet, A diverse enhanced capsule network with disperse dynamic routing, Appl. Sci. 10 (3) (2020) 884.
[38] H. Ren, J. Su, H. Lu, Evaluating Generalization Ability of Convolutional Neural Networks and Capsule Networks for Image Classification via Top-2 Classification, 2019 *arXiv preprint arXiv*:1901.10112.
[39] S. Yang, F. Lee, R. Miao, J. Cai, L. Chen, W. Yao, K. Kotani, Q. Chen, Rs-CapsNet, An advanced capsule network, IEEE Access 8 (2020) 85007–85018.
[40] A. Saif, T. Imtiaz, S. Rifat, C. Shahnaz, W.-P. Zhu, M.O. Ahmad, CapsCovNet: a modified capsule network to diagnose Covid-19 from multimodal medical imaging, IEEE Trans. Artif. Intell. 2 (6) (2021) 608–617.
[41] H. Quan, X. Xu, T. Zheng, Z. Li, M. Zhao, X. Cui, DenseCapsNet: detection of COVID-19 from X-ray images using a capsule neural network, Comput. Biol. Med. 133 (2021), 104399.
[42] P. Gupta, M.K. Siddiqui, X. Huang, R. Morales-Menendez, H. Pawar, H. Terashima-Marin, M.S. Wajid, COVID-WideNet—a capsule network for COVID-19 detection, Appl. Soft Comput. 122 (2022), 108780.
[43] F. Li, X. Lu, J. Yuan, MHA-CoroCapsule: multi-head attention routing-based capsule network for COVID-19 chest X-ray image classification, IEEE Trans. Med. Imag. 41 (5) (2021) 1208–1218.
[44] K. Zhang, X. Liu, J. Shen, Z. Li, Y. Sang, X. Wu, Y. Zha, W. Liang, C. Wang, K. Wang, Clinically applicable AI system for accurate diagnosis, quantitative measurements, and prognosis of COVID-19 pneumonia using computed tomography, Cell 181 (6) (2020) 1423–1433.
[45] K. Clark, B. Vendt, K. Smith, J. Freymann, J. Kirby, P. Koppel, S. Moore, S. Phillips, D. Maffitt, M. Pringle, The Cancer Imaging Archive (TCIA): maintaining and operating a public information repository, J. Digit. Imag. 26 (6) (2013) 1045–1057.
[46] A. Chaurasia, E. Culurciello, Linknet: exploiting encoder representations for efficient semantic segmentation, in: 2017 IEEE Visual Communications and Image Processing (VCIP), IEEE, 2017, pp. 1–4.
[47] O. Ronneberger, P. Fischer, T. Brox, U-net, Convolutional networks for biomedical image segmentation, in: International Conference on Medical Image Computing and Computer-Assisted Intervention, Springer, 2015, pp. 234–241.
[48] K. He, X. Zhang, S. Ren, J. Sun, Deep residual learning for image recognition, in: Proceedings of the IEEE Conference on Computer Vision and Pattern Recognition, 2016, pp. 770–778.
[49] L. Fei-Fei, J. Deng, K. Li, ImageNet: constructing a large-scale image database, J. Vis. 9 (8) (2009), 1037-1037.
[50] M.Z. Alom, C. Yakopcic, M. Hasan, et al., Recurrent residual U-Net for medical image segmentation[J], J. Med. Imaging 6 (1) (2019), 014006.
[51] O. Oktay, J. Schlemper, L.L. Folgoc, M. Lee, M. Heinrich, K. Misawa, K. Mori, S. McDonagh, N.Y. Hammerla, B. Kainz, Attention U-Net: Learning where to Look for the Pancreas, 2018 *arXiv preprint arXiv:1804.03999*.
[52] Z. Zhou, M.M.R. Siddiquee, N. Tajbakhsh, J. Liang, Unet++: a nested u-net architecture for medical image segmentation, in: Deep Learning in Medical Image Analysis and Multimodal Learning for Clinical Decision Support, Springer, 2018, pp. 3–11.
[53] Z. Zhou, M.M.R. Siddiquee, N. Tajbakhsh, J. Liang, Unet++: redesigning skip connections to exploit multiscale features in image segmentation, IEEE Trans. Med. Imag. 39 (6) (2019) 1856–1867.
[54] H. Shaziya, K. Shyamala, R. Zaheer, Automatic lung segmentation on thoracic CT scans using U-Net convolutional network, in: 2018 International Conference on Communication and Signal Processing (ICCSP), IEEE, 2018, 0643-0647.
[55] E. İn, A.A. Geçkil, G. Kavuran, M. Şahin, N.K. Berber, M. Kuluöztürk, Using artificial intelligence to improve the diagnostic efficiency of pulmonologists in differentiating COVID-19 pneumonia from community-acquired pneumonia, J. Med. Virol. 94 (8) (2022) 3698–3705.
[56] F. Xu, K. Lou, C. Chen, Q. Chen, D. Wang, J. Wu, W. Zhu, W. Tan, Y. Zhou, Y. Liu, An original deep learning model using limited data for COVID-19 discrimination: a multicenter study, Med. Phys. 49 (6) (2022) 3874–3885.
[57] T. Javaheri, M. Homayounfar, Z. Amoozgar, R. Reiazi, F. Homayounieh, E. Abbas, A. Laali, A.R. Radmard, M.H. Gharib, S.A.J. Mousavi, CovidCTNet: an open-source deep learning approach to diagnose covid-19 using small cohort of CT images, NPJ Dig. Med. 4 (1) (2021) 29.
[58] Q. Zhu, Y. Zhou, Y. Yao, L. Sun, F. Shi, W. Shao, D. Zhang, D. Shen, Semi-supervised multi-view fusion for identifying CAP and COVID-19 with unlabeled CT images, IEEE Trans. Emerg. Topics Comput. Intell. (2022) 1–13.
[59] J. Song, H. Wang, Y. Liu, W. Wu, G. Dai, Z. Wu, P. Zhu, W. Zhang, K.W. Yeom, K. Deng, End-to-end automatic differentiation of the coronavirus disease 2019 (COVID-19) from viral pneumonia based on chest CT, Eur. J. Nucl. Med. Mol. Imag. 47 (11) (2020) 2516–2524.
[60] M. Abdel-Basset, H. Hawash, N. Moustafa, O.M. Elkomy, nnTwo-stage deep learning framework for discrimination between COVID-19 and community-acquired pneumonia from chest CT scans, Pattern Recogn. Lett. 152 (2021) 311–319.
[61] L. Li, L. Qin, Z. Xu, Y. Yin, X. Wang, B. Kong, J. Bai, Y. Lu, Z. Fang, Q. Song, Using artificial intelligence to detect COVID-19 and community-acquired pneumonia based on pulmonary CT: evaluation of the diagnostic accuracy, Radiology 296 (2) (2020) E65–E71.
[62] L. Van der Maaten, G. Hinton, Visualizing data using t-SNE, J. Mach. Learn. Res. 986 (2008) 2579–2605.
[63] Y. Qiblawey, A. Tahir, M.E. Chowdhury, A. Khandakar, S. Kiranyaz, T. Rahman, N. Ibtehaz, S. Mahmud, S.A. Maadeed, F. Musharavati, Detection and severity classification of COVID-19 in CT images using deep learning, Diagnostics 11 (5) (2021) 893.
[64] S.P. Pawar, S.N. Talbar, LungSeg-Net: lung field segmentation using generative adversarial network, Biomed. Signal Process Control 64 (2021), 102296.
[65] M. Osadebey, H.K. Andersen, D. Waaler, K. Fossaa, A.C. Martinsen, M. Pedersen, Three-stage segmentation of lung region from CT images using deep neural networks, BMC Med. Imag. 21 (1) (2021) 112.
[66] H. Xie, H. Shan, W. Cong, C. Liu, X. Zhang, S. Liu, R. Ning, G. Wang, Deep efficient end-to-end reconstruction (DEER) network for few-view breast CT image reconstruction, IEEE Access 8 (2020) 196633–196646.
[67] D.J. Brenner, E.J. Hall, Computed tomography—an increasing source of radiation exposure, N. Engl. J. Med. 357 (22) (2007) 2277–2284.
[68] R. Subhalakshmi, S.A.A. Balamurugan, S. Sasikala, Deep learning based fusion model for COVID-19 diagnosis and classification using computed tomography images, Concurr. Eng. Res. Appl. 30 (1) (2022) 116–127.
[69] H.K. Bhuyan, C. Chakraborty, Y. Shelke, S.K. Pani, COVID-19 diagnosis system by deep learning approaches, Expet Syst. (2021), e12776.
[70] Y. Kim, M.-J. Lee, M.-J. Kim, Comparison of Radiation Dose from X-Ray, CT, and PET/CT in Paediatric Patients with Neuroblastoma Using a Dose Monitoring Program, European Congress of Radiology-ECR, 2015, 2015.
[71] M. Chung, A. Bernheim, X. Mei, N. Zhang, M. Huang, X. Zeng, J. Cui, W. Xu, Y. Yang, Z.A. Fayad, CT imaging features of 2019 novel coronavirus (2019-nCoV), Radiology 295 (1) (2020) 202–207.
[72] T.S. Fung, D.X. Liu, Similarities and dissimilarities of COVID-19 and other coronavirus diseases, Annu. Rev. Microbiol. 75 (1) (2021) 1–29.
[73] M. Abdel-Basset, H. Hawash, N. Moustafa, O.M. Elkomy, Two-stage deep learning framework for discrimination between COVID-19 and community-acquired pneumonia from chest CT scans, Pattern Recogn. Lett. 152 (2021) 311–319.
[74] E.-A. Park, J.M. Goo, J.W. Lee, C.H. Kang, H.J. Lee, C.H. Lee, C.M. Park, H.Y. Lee, J.-G. Im, Efficacy of computer-aided detection system and thin-slab maximum intensity projection technique in the detection of pulmonary nodules in patients with resected metastases, Invest. Radiol. 44 (2) (2009) 105–113.
[75] P. Monkam, S. Qi, H. Ma, W. Gao, Y. Yao, W. Qian, Detection and classification of pulmonary nodules using convolutional neural networks: a survey, IEEE Access 7 (2019) 78075–78091.
[76] B. Zhang, S. Qi, P. Monkam, C. Li, F. Yang, Y.-D. Yao, W. Qian, Ensemble learners of multiple deep CNNs for pulmonary nodules classification using CT images, IEEE Access 7 (2019) 110358–110371.